Proceedings of Global Power and Propulsion Society
ISSN-Nr: 2504-4400
GPPS Xi'an21
18th–20th October, 2021

www.gpps.global

GPPS-TC-2021-0192

Analysis of Wheel Space Ingress in a One-Stage Axial Turbine

Thomas Hösgen
Institute of Aerodynamics
RWTH Aachen University
t.hoesgen@aia.rwth-aachen.de
Aachen, Germany

Matthias H. Meinke
Institute of Aerodynamics
RWTH Aachen University
m.meinke@aia.rwth-aachen.de
Aachen, Germany

Wolfgang Schröder
Institute of Aerodynamics
RWTH Aachen University
office@aia.rwth-aachen.de
Aachen, Germany

ABSTRACT

The ingress of main annulus gas into the wheel space of an one-stage axial flow turbine with 30 stator and 62 rotor blades is analyzed based on the results of a large-eddy simulation (LES) of the full 360° circumference of the turbine stage. The Navier-Stokes equations are solved using a finite-volume solver based on a Cartesian mesh with cut cells for the wall surfaces. The rotating blades are tracked by a level set, which is transported with a semi-Lagrangian method. The cut cell formulation at the boundaries with a flux redistribution method ensures conservation of mass, momentum, and energy. The LES is performed for a low cooling gas mass flow rate, at which several acoustic modes are excited in the wheel space. The focus of the analysis is on the determination of the main annulus gas ingress contributed by the various modes. For that purpose, the radial velocity component is filtered at the frequencies of the various modes and the time and azimuthally averaged main annulus gas ingress is computed as a function of the individual modes of the radial velocity fluctuations. The results show that the acoustic modes generating the largest amplitude of radial velocity fluctuations do not cause substantial ingress. This can be attributed to the relatively long time scale of the turbulent mixing of main annulus gas with the cooling gas compared to the time scale of the acoustic modes. Only modes at low frequencies generate substantial ingress, which is confirmed by the energy spectra of main annulus gas concentration variations.

INTRODUCTION

By optimizing the thermal efficiency of turbomachinery the emission of polutants and the amount of primary energy used by the transport and energy sector can be reduced. One means to improve the thermal efficiency of gas turbines, is increasing the turbine inlet temperature. The higher thermal loads due to the increased temperature, however, result in immense challenges in the design of turbine cooling systems. This also includes the unavoidable wheel space between the stator and the rotor disks. Hot gas from the outer main annulus flow that enters the wheel space through the rim seal gap enhances the thermal loads on the stator and rotor disks, which reduces the turbine life span. To prevent ingress of main annulus gas into the wheel space, cooling gas from the turbine's secondary air system is introduced into the wheel space. The cooling air serves as sealing gas in the rim seal gap and cools the stator and rotor disks. Since providing the cool gas decreases the turbine's efficiency, sophisticated rim seal geometries are developed to minimize the necessary amount of cooling gas. This requires a profound knowledge of the flow inside the rim seal.

Inside the wheel space, the disk pumping effect of the rotor disk accelerates the cooling gas in the circumferential and radial direction. (Johnson et al., 1994). In the rim seal gap, the cooling gas interacts with the main annulus flow, i.e., a shear layer exists because of the different velocities of the cooling gas and the main annulus flow, and further, pressure fluctuations caused by rotor stator interactions propagate into the rim seal gap. This creates a highly complex, three- dimensional and unsteady flow in the rim seal gap. When exiting the rim seal gap into the main annulus, these complex flow strucures affect the secondary flow structures of the main annulus flow (Schuepbach et al., 2010) and (Schädler et al., 2016) and, moreover, they can transport more main annulus gas into the wheel space, i.e., reduce the sealing effectiveness.

To evaluate the quality of rim seal geometries, i.e., sealing effectiveness, by use of numerical simulations, the correct prediction of these unsteady flow phenomena is essential. For instance, (Horwood et al., 2018, 2020) compared data from unsteady Reynolds-Averaged Navier-Stokes (URANS)-simulations to experimental results for different wheel space geometries and evidenced that for some cooling gas mass flow rates the URANS underestimates the hot gas ingress. This deviation was suspected to be related to strong pressure fluctuations, which were measured but not captured in the numerical

data. (Laskowski et al., 2009), further, compared the results of steady-state RANS simulations to results of unsteady RANS simulations of a turbine model with simplified rotor blading. The comparison showed considerably better agreement of the unsteady data with experimental data than for the steady-state results. The unsteady RANS predicted Kelvin-Helmholtz fluctuations in the shear layer inside the rim seal gap even with neglected rotor rotation. Similar structures were found by (Rabs et al., 2009), when simulating a 1.5-stage axial turbine without blading, which were significantly reduced when blades were added.

The structure of the observed large scale unsteady flow phenomena depends on several factors such as the rim seal geometry (Chilla et al., 2013) and the rotor speed (Beard et al., 2016). Further, several authors, e.g., (Beard et al., 2016), (Bohn et al., 2003) and (Rudzinski, 2009), reported an influence of the cooling gas mass flow rate on the unsteady flow. (Bohn et al., 2003) and (Rudzinski, 2009) measured pressure fluctuations inside the rim seal, which strongly affected the sealing effectiveness and which frequencies were unrelated to the blade passing frequency (BPF). The unsteady phenomena only existed in a certain range of cooling gas mass flow rates, which is in agreement of the findings of (Horwood et al., 2018, 2020). Outside this range, the fluctuations vanished abruptly. Recently, (Iranidokht et al., 2021) were able to affect the amplitudes and the frequencies of cavity modes observed on their test rig by modifying the wheel space geometry.

The large number of influencing factors renders the numerical simulations of the unsteady flow challenging. Moreover, it is difficult to estimate the effects of certain simplifications such as the application of a sector model. For example, (Jakoby et al., 2004) conducted numerical simulations of the 1.5-stage turbine, which has been experimetally investigated by (Bohn et al., 2003) and (Rudzinski, 2009), for multiple sector sizes and a full 360° simulation. They observed that only the 360° simulation predicted a rotating mode inside the wheel space, which was supressed in the sector computations due to the insufficient sector size. Similar, (Cao et al., 2004) observed periodic structures inside the rim seal where the number of lobes depended on the sector size.

The numerical simulations are commonly based on the RANS approach. The commonly used turbulence models seem, however, to not be able to accurately desrcibe the turbulent flow field. (O'Mahoney et al., 2010) carried out a large-eddy simulation (LES), which requires less modelling and compared the results obtained for a small sector model to URANS and experimental data. The LES results showed better agreement with the experimental data than the URANS solution.

The capability of LES to accurately predict the complex flow field in the wheel space and rim seal has been shown by (Pogorelov et al., 2019). They used LES to investigate the full 360° circumference of an axial flow turbine including the main annulus and the wheel space. For a setup with a single lip rim seal, Kelvin-Helmholtz fluctuations were found in the shear layer between main annulus flow and cooling gas. These fluctuations interacted with the main annulus flow and led to an increased ingress. When a second sealing lip was added to the rim seal, the fluctuations were supressed, which increased the sealing effectiveness. The same double lip rim seal was later investigated by (Hösgen et al., 2020) for a reduced cooling mass flow rate. One important finding was the occurrence of standing acoustic waves, where the frequencies coincide with acoustic modes of the wheel space.

In this paper, the results from (Hösgen et al., 2020) are further analyzed to determine the net ingress due to the various modes observed in the simulations. The paper is organized as follows. First, the governing equations and the numerical approach are discussed. Second, the computational setup and the investigated operating condition are presented. Subsequently, the analyses for the ingress of hot gas are summarized based on the filtered velocity signals at the frequencies of the observed modes at the upper and lower lip of the rim seal. Finally, some conclusions are drawn.

METHODOLOGY

Numerical Method

The LES results are obained using the in-house flow sovler m-AIA. This numerical method solves the compressible Navier-Stokes equations for an ideal gas in the absolute frame of reference. The sub-grid scales are determined using the monotone integrated LES (MILES) approach (Boris et al., 1992). A modified version of the advection upstream splitting method (AUSM) proposed by (Meinke et al., 2002) is used to compute the inviscid flux. The viscous flux is obtained with a central-difference scheme. Time-integration is carried out using the explicit second-order accurate 5-stage Runge-Kutta scheme of (Schneiders et al., 2016), which has been developed specifically for the simulation of moving boundaries. The movement of the rotor is prescribed by a multi-level-set method (Günther et al., 2014). The conservation of mass, momentum, and energy at the walls is ensured by an strictly conservative cut-cell method (Schneiders et al., 2016). More details regarding the numerical method can be found in Hösgen et al. (2020).

COMPUTATIONAL SETUP

The analysis is based on the flow field in the one-stage axial turbine depicted in Figure 1. The stator row consists of 30 vanes and the rotor has 62 blades. The rim seal, shown in Figure 2, consists of two seal lips, where the upper lip is mounted on the stator disk and the lower lip is mounted on the rotor disk.

The computational mesh has approximately 450 million cells and includes the full 360° circumference of the main annulus flow and the wheel space. For more detailed information on the computational grid and the imposed boundary conditions the reader is referred to (Hösgen et al., 2020).

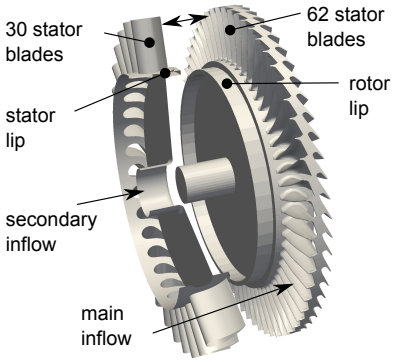

Figure 1 Cut through the one-stage axial flow turbine; rotor and stator are separated (Hösgen et al., 2020).

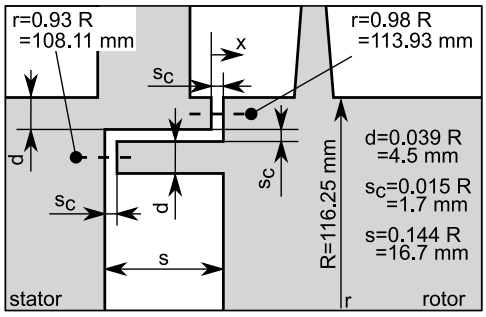

Figure 2 Schematic view of the rim seal geometry (Hösgen et al., 2020).

The operating condition is defined by the four dimensionless quantities given in Table 1. The two subscripts, 1 and cg denote the flow state $0.013 \cdot R$ downstream of the stator blades and at the cooling gas inlet.

Table 1 Operating condition.

Main flow Reynolds number	$Re_{c_1} = \rho_1 c_1 R/\mu_1$	$0.8 \cdot 10^6$
Main flow Mach number	$M_{c_1} = c_1/\sqrt{\gamma R T_1}$	0.37
Rotational Reynolds number	$Re_u = \rho_{cg} \Omega R^2/\mu_{cg}$	$0.8 \cdot 10^6$
Dimensionless cooling gas mass flux	$cw = \dot{m}_{cg}/\mu_{cg} R$	1000

RESULTS AND DISCUSSION

In (Hösgen et al., 2020) simulation results of the flow field in the one-stage axial flow turbine have been discussed in detail for two cooling gas mass flow rates, i.e., $cw = 1000$ and $cw = 2000$. Good agreement of the cooling efficiency with experimental data has been shown in both cases. In the following, the ingress of the main annulus gas for the case with the lower cooling gas mass flux, i.e., $cw = 1000$, is analyzed in more detail by determining the mass flow rates of the main annulus gas ingress associated to various modes observed in the wheel space and the rim seal gap of the one stage axial turbine. This analysis is based on the simulation results after approximately 40 full rotor rotations, when a fully developed flow field is established also in the wheel space. Time resolved data for the flow variables were recorded at the outer and inner lip of the rim seal for about 1.5 rotations of the rotor in several distinct locations with 0.2 degree spacing in the circumferential direction and at a time interval of $\Delta t/n = 5.5 \cdot 10^{-4}$ such that a sample is taken each 0.2 degree rotation of the rotor. All variables were averaged along the seal gap width s_c in the axial direction.

The results in (Hösgen et al., 2020) showed peaks in the fluctuations of the radial velocity component at various acoustic modes of the wheel space. The spectrum of the radial velocity component averaged in the circumferential direction is shown in Figure 3 and the acoustic modes are summarized in Table 2 in comparison to the harmonics of a closed pipe with comparable characteristic length $L = R - (2 \cdot d + s_c) - r_b$ as the radius of the wheel space. The quantity r_b is the radius of the rotor shaft. More details can be found in (Hösgen et al., 2020).

Table 2 Harmonics of a closed pipe and the modes observed in the radial velocity spectra normalized by the rotor speed (Hösgen et al., 2020).

Mode No.	7	8	11	12	13	16	17	18	21	24
Pipe f/n	84.17	96.20	132.27	144.29	156.32	192.39	204.42	216.44	252.51	288.59
LES f/n	79.53	94.33	126.6	141.5	156.3	188.7	203.5	218.3	250.6	283.1
Rel. Error	-5.5 %	-1.9 %	4.2 %	-1.9 %	-0.01 %	-1.9 %	-0.5 %	0.9 %	-0.8 %	-1.9 %

In the following, the contribution to the main annulus gas ingress of individual modes is analyzed. The radial velocity fluctuations v_r' are computed from the velocity signal recorded in the rim seal gap. To obtain the radial velocity fluctuations that correspond to a certain mode, the fluctuations are filtered at the frequency of the respective mode using a 4^{th}-order butterworth bandpass filter. This way, the contribution $v_{r,m}'$ of a mode m to the raw velocity fluctuations v_r' is determined. The magnitude and the phase response of the filter applied at the frequency $f/n = 126$ are displayed in Figure 4. The lower and upper cut-off frequencies are chosen to $f_{cut-off}/n = 126 \pm 3$. In the frequency domain, the amplitudes of the discrete

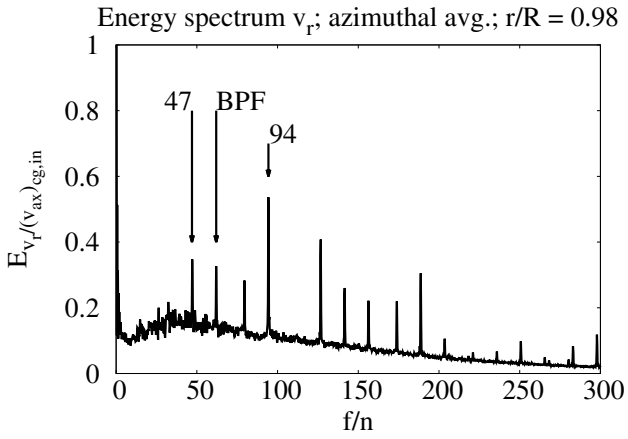

Figure 3 Spectra of the radial velocity fluctuations averaged in the circumferential direction at $r/R = 0.98$, i.e., the outer rim seal gap.

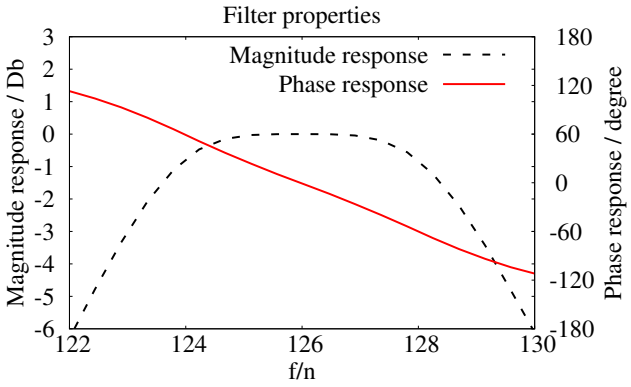

Figure 4 Magnitude and phase response of the applied bandpass filter at the distinct frequency $f/n = 126$.

frequencies outside the passband, i.e., below or above the cut-off frequencies, are damped by more than 3 dB by the filter. Further frequencies away from the filter frequency $f_m/n = 126$ in the center of the passband experience a phase shift, which results in a distortion of the signal after it is transformed back into the time domain. The cut-off frequencies are chosen such that a sharp filter is achieved, while distortions of the filtered signal due the phase shift are kept small. Hence, the filtered signal contains a range of discrete frequencies rather than a distinct frequency.

Using the filtered fluctuations of the radial velocity component $v'_{r,m}$, the main annulus gas mass flow rate $\dot{m}_{hg,m}$ through the sealing gap associated to a certain frequency range can be computed by

$$\dot{m}_{hg,m} = \int_{\theta=0}^{2\pi} \frac{1}{1.5T} \int_{t=0}^{1.5T} \rho\, Y_{hg}\, v'_{r,m}\, dt\, s_c R\, d\theta \quad , \tag{1}$$

where 1.5 T corresponds to the 1.5 rotations rotor, for which data was sampled. The quantity ρ is the instantaneous density and Y_{hg} is the main annulus gas concentration.

The ingress and the concentration flux of the main annulus gas $v'_{r,m}Y_{hg}$ as a function of filter frequency are shown in Figure 5. Here, the main annulus gas mass flow rate $\dot{m}_{hg,m}$ was computed by continously shifting the filter frequency f_m/n from low to high values.

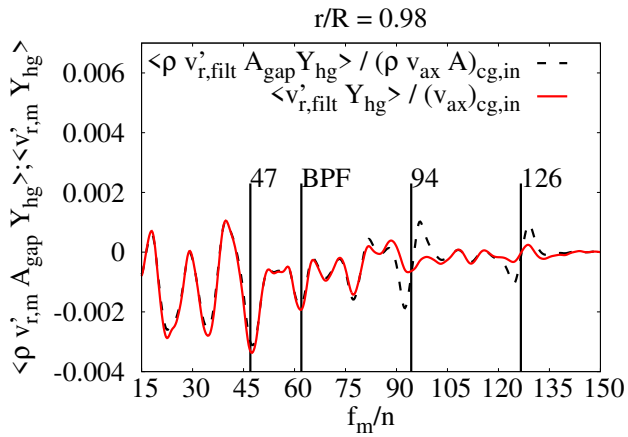

Figure 5 Modal decomposition of the ingress mass flux and the main annulus gas concentration flux at the outer rim seal gap ($r/R = 0.98$). Negative values indicate ingress into the wheel space.

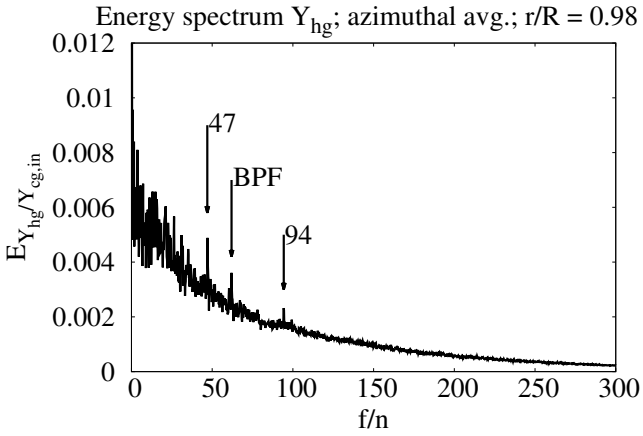

Figure 6 Spectra of the fluctuations of the main annulus gas concentration Y'_{hg} averaged in circumferential direction at $r/R = 0.98$, i.e., the outer rim seal gap.

The mass flux variations around the frequencies $f_m/n = 94$ and $f_m/n = 126$ are discussed first. In general, a pure acoustic standing wave generates velocity and density modes at the same frequency with a phase shift of $\phi = \pi/2$ such that the resulting mass flux being the product of the velocity and density integrated over time is zero. Although standing acoustic waves at $f/n = 94$ and higher frequencies are observed in the wheel space, the integrated mass flux shows symmetric peaks

of ingress and egress around these particular frequencies. This, however, is an artefact of the filter operation. For modes with frequencies in the range of $f_m/n = 94 \pm 3$ the dominant mode at $f/n = 94$ lies inside the passband of the filter and experiences a phases shift. The altered phase difference between the reconstructed radial velocity fluctuations $v'_{r,m}$ and the unfiltered density ρ results in a positive or negative mass flux around the acoustic modes, and vanishes at $f_m/n = 94$. If a sharper filter is used, i.e., when the cut-off frequencies are set to $f_{cut-off}/n = f_m/n \pm 2$, the peaks move closer to $f_m/n = 94$, however, the amplitudes increase. For the concentration flux $v'_{r,m}Y_{hg}$, these artificial peaks do not appear, since no significant mode amplitude of the concentration fluctuations exists at this frequency. From the mode decomposition at $f/n = 94$ of the density and radial velocity fluctuations, a phase difference of $\Delta\phi = 0.56\pi$ is determined from the LES results, which is close to the theoretical value for a standing wave.

Ingress of the main annulus gas can occur when the main annulus gas concentration fluctuations defined by Y'_{hg} show significant variations where also modes of velocity fluctuations exist. The energy spectrum of the radial velocity fluctuations v'_r averaged in the circumferential direction in Figure 3 shows the mode with the highest amplitude to be at $f/n = 94$. From Figure 5 it is evident that this dominant mode only results in a minor transport of main annulus gas into the wheel space. Since concentration variations are mainly caused by the turbulent fluctuations at a convective time scale, which appear mainly below $t \cdot n = 1/94$, no significant concentration variations can be generated at the higher frequencies of the observed acoustic waves. Therefore, modes at $f/n \geq 94$ only contribute marginally to the main annulus flow ingress. This is also confirmed by the circumferentially averaged energy spectrum of the main annulus gas concentration Y_{hg} at the upper sealing lip in Figure 6. The spectrum only shows a minor peak at $f/n = 94$ and no mode amplitudes at higher frequencies.

Figure 5 shows that the ingress at the outer sealing lip at $r/R = 0.98$ mainly occurs at the modes $f/n = 47$, $f/n =$BPF$=$ 62 and, additionally, at lower frequent modes. The exact frequencies of the two lower modes cannot be accurately determined based on the short averaging interval of 1.5 rotations. They are approximately $f/n \approx 22$ and $f/n \approx 35$, which could be subharmonics of $f/n = 47$ and the BPF. These two modes are especially interesting, since they do not appear as high amplitude modes in the energy spectrum of the radial velocity fluctuations in Figure 3. This analysis, however, shows that they have a major impact on the main annulus gas ingestion. Hence, these results suggest that ingress in this axial turbine stage setup is not driven by the modes with the largest amplitudes of velocity or pressure fluctuations such that a tuning of the wheel space geometry as suggested by (Iranidokht et al., 2021) to reduce these mode amplitudes does not necessarily result in a better cooling effectivenss.

Next, the results for the in- and egress of main annulus gas at the inner lip at $r/R = 0.93$ shown in Figure 7 are discussed. In general, the peaks of in- or egress are of much lower amplitude than for the outer seal lip. Similar to the

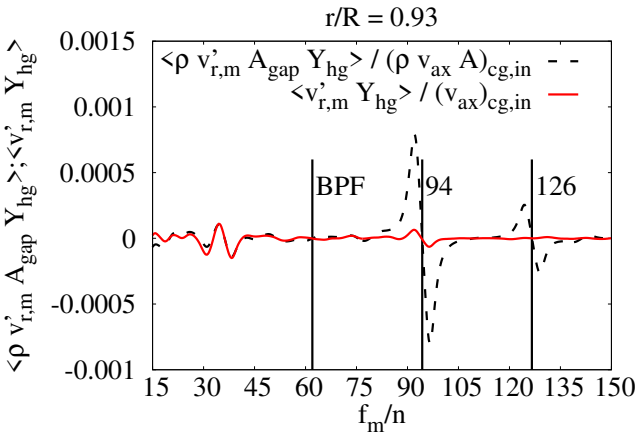

Figure 7 Modal decomposition of the ingress mass flux and the main annulus gas concentration flux at the inner rim seal gap ($r/R = 0.93$). Negative values indicate ingress into the wheel space.

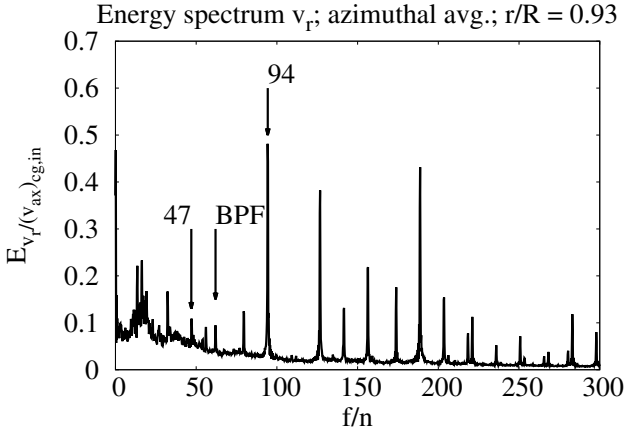

Figure 8 Spectra of the radial velocity fluctuations averaged in circumferential direction at $r/R = 0.93$, i.e., the inner rim seal gap.

results for the outer sealing lip, the integrated mass flux shows artificial peaks due to the non-perfect bandpass filtering around the frequencies $f_m/n = 94$ and $f_m/n = 126$. Non-zero ingress can only be observed at the modes $f_m/n \approx 31$ and $f_m/n \approx 40$, where again the exact determination of this modes needs additional time samples. No significant main annulus gas ingress is observed at any of the various high amplitude modes of the radial velocity fluctuations, clearly discernable in the energy spectrum of v'_r depicted in Figure 8.

Although the short sampling interval does not allow an exact determination of the ingress at low frequencies, the analysis shows that the ingress of the main annulus gas at the lower sealing lip seems to occur at frequencies of $f/n = 40$ and lower, where the energy spectrum of the radial velocity fluctuations does not show significant mode peaks.

CONCLUSIONS

A modal analysis of the main annulus gas ingress into the wheel space of a one-stage axial flow turbine was performed based on results of a large-eddy simulation for an operating condition with a small cooling gas mass flow rate. For this operating condition, several acoustic modes are excited. The modal analysis of the ingress of the main annulus gas shows that modes at high frequency, i.e., $f/n \geq 94$ do not generate significant ingress. This can be attributed to the relatively long time scale of the turbulent mixing of the main annulus and the cooling gas at a convective time scale, compared to the time scale of the acoustic modes. This is confirmed by the results of the energy spectra for the concentration fluctuations, which shows only 3 distinct modes at frequencies lower than the most dominant acoustic mode. Further analyses will be performed to reveal the detailed mechanism of the low frequent modes at which the largest ingress is observed.

NOMENCLATURE

Symbol	
BPF	Blade passing frequency
c	Velocity in main flow direction
cw	Dimensionless cooling gas mass flow rate
d	Width of rim seal lip
f	Frequency
$f_{cut-off}$	Filter cut-off frequency
f_m	Filter frequency
LES	Large-eddy simulation
M_{c_1}	Main flow Mach number
$\dot{m}_{cg}$	Cooling gas mass flow rate
$\dot{m}_{hg,m}$	Main annulus gas mass flux asscociated to frequency m
n	Rotor speed (Hz)
R	Rotor hub radius
RANS	Reynolds-Averaged Navier-Stokes
Re_{c_1}	Main flow Reynolds number
Re_u	Rotational Reynolds number
r_b	Radius of rotor shaft
s	Axial with of wheel space
s_c	Axial with of rim seal gap
T	Temperature
T	Time needed for one full rotor rotation $(1/n)$
Δt	Time step size
v'_r	Radial velocity fluctuations
$v'_{r,m}$	Filtered radial velocity fluctuations at frequency m
Y_{hg}	Main annulus gas concentration
γ	Ratio of specific heats
μ	Dynamic viscosity
ρ	Density
Ω	Rotor speed (rad/s)

ACKNOWLEDGMENTS

The authors gratefully acknowledge the Gauss Centre for Supercomputing e.V. (www.gauss-centre.eu) for funding this project by providing computing time on the GCS Supercomputer HAWK at Höchstleistungsrechenzentrum Stuttgart (www.hlrs.de).

The research project was performed in the framework of the industrial collective research programme (IGF No. 19198N). It was supported by the Federal Ministry for Economic Affairs and Energy (BMWi) through the AiF (German Federation of Industrial Research Associations eV) based on a decision taken by the German Bundestag.

References

Beard, P. F., Gao, F., Chana, K. S. and Chew, J. (2016), 'Unsteady flow phenomena in turbine rim seals', *Journal of Engineering for Gas Turbines and Power* **139**(3).

Bohn, D., Decker, A., Ma, H. and Wolff, M. (2003), Influence of sealing air mass flow on the velocity distribution in and

inside the rim seal of the upstream cavity of a 1.5-stage turbine, *in* 'Volume 5: Turbo Expo 2003, Parts A and B', Turbo Expo: Power for Land, Sea, and Air, pp. 1033–1040.

Boris, J. P., Grinstein, F. F., Oran, E. S. and Kolbe, R. L. (1992), 'New insights into large eddy simulation', *Fluid Dynamics Research* **10**(4), 199–228.

Cao, C., Chew, J. W., Millington, P. R. and Hogg, S. I. (2004), 'Interaction of rim seal and annulus flows in an axial flow turbine', *Journal of Engineering for Gas Turbines and Power* **126**(4), 786–793.

Chilla, M., Hodson, H. and Newman, D. (2013), 'Unsteady interaction between annulus and turbine rim seal flows', *Journal of Turbomachinery* **135**(5).

Günther, C., Meinke, M. and Schröder, W. (2014), 'A flexible level-set approach for tracking multiple interacting interfaces in embedded boundary methods', *Computers & Fluids* **102**, 182–202.

Horwood, J. T. M., Hualca, F. P., Scobie, J. A., Wilson, M., Sangan, C. M. and Lock, G. D. (2018), 'Experimental and Computational Investigation of Flow Instabilities in Turbine Rim Seals', *Journal of Engineering for Gas Turbines and Power* **141**(1).

Horwood, J. T. M., Hualca, F. P., Wilson, M., Scobie, J. A., Sangan, C. M., Lock, G. D., Dahlqvist, J. and Fridh, J. (2020), 'Flow Instabilities in Gas Turbine Chute Seals', *Journal of Engineering for Gas Turbines and Power* **142**(2).

Hösgen, T., Meinke, M. and Schröder, W. (2020), 'Large-eddy simulations of rim seal flow in a one-stage axial turbine', *Journal of the Global Power and Propulsion Society* **4**, 309–321.

Iranidokht, V., Kalfas, A. I., Abhari, R. S., Senoo, S. and Momma, K. (2021), 'Sensitivity analysis on the impact of geometrical and operational variations on turbine hub cavity modes and practical methods to control them', *Journal of the Global Power and Propulsion Society* **5**, 66–78.

Jakoby, R., Zierer, T., Lindblad, K., Larsson, J., deVito, L., Bohn, D. E., Funcke, J. and Decker, A. (2004), Numerical simulation of the unsteady flow field in an axial gas turbine rim seal configuration, *in* 'Volume 4: Turbo Expo 2004', Turbo Expo: Power for Land, Sea, and Air, pp. 431–440.

Johnson, B. V., Mack, G. J., Paolillo, R. E. and Daniels, W. A. (1994), 'Turbine rim seal gas path flow ingestion mechanisms', *AIAA Paper 94-2703* .

Laskowski, G. M., Bunker, R. S., Bailey, J. C., Ledezma, G., Kapetanovic, S., Itzel, G. M., Sullivan, M. A. and Farrell, T. R. (2009), An investigation of turbine wheelspace cooling flow interactions with a transonic hot gas path—part 2: Cfd simulations, *in* 'Volume 3: Heat Transfer, Parts A and B', Turbo Expo: Power for Land, Sea, and Air, pp. 1095–1111.

Meinke, M., Schröder, W., Krause, E. and Rister, T. (2002), 'A comparison of second- and sixth-order methods for large-eddy simulations', *Computers & Fluids* **31**(4), 695–718.

O'Mahoney, T. S. D., Hills, N. J., Chew, J. W. and Scanlon, T. (2010), Large-eddy simulation of rim seal ingestion, *in* 'Volume 4: Heat Transfer, Parts A and B', Turbo Expo: Power for Land, Sea, and Air, pp. 1155–1165.

Pogorelov, A., Meinke, M. and Schröder, W. (2019), 'Large-eddy simulation of the unsteady full 3d rim seal flow in a one-stage axial-flow turbine', *Flow, Turbulence and Combustion* **102**(1), 189–220.

Rabs, M., Benra, F.-K., Dohmen, H. J. and Schneider, O. (2009), Investigation of flow instabilities near the rim cavity of a 1.5 stage gas turbine, *in* 'Volume 3: Heat Transfer, Parts A and B', Turbo Expo: Power for Land, Sea, and Air, pp. 1263–1272.

Rudzinski, B. (2009), *Experimentelle Untersuchung des Heißgaseinzuges in die Rotor-Stator-Zwischenräume einer eineinhalbstufigen Turbine für unterschiedliche Dichtkonfigurationen: Zugl.: RWTH Aachen University, Diss., 2009*, Verlag Dr. Hut, München.

Schädler, R., Kalfas, A. I., Abhari, R. S., Schmid, G. and Voelker, S. (2016), 'Modulation and radial migration of turbine hub cavity modes by the rim seal purge flow', *Journal of Turbomachinery* **139**(1).

Schneiders, L., Günther, C., Meinke, M. and Schröder, W. (2016), 'An efficient conservative cut-cell method for rigid bodies interacting with viscous compressible flows', *Journal of Computational Physics* **311**, 62–86.

Schuepbach, P., Abhari, R. S., Rose, M. G., Germain, T., Raab, I. and Gier, J. (2010), 'Effects of suction and injection purge-flow on the secondary flow structures of a high-work turbine', *Journal of Turbomachinery* **132**(2).